

Conductance Switching and Inhomogeneous Field Melting in the Charge Ordered Manganites

ANAMITRA MUKHERJEE, KALPATARU PRADHAN and PINAKI MAJUMDAR

Harish-Chandra Research Institute, Chhatnag Road, Jhusi, Allahabad 211019, India

PACS 75.47.Lx – Manganites
 PACS 71.27.+a – Strongly correlated electron systems
 PACS 75.30.Kz – Magnetic phase boundaries

Abstract. - The field induced switching of conductance in the charge ordered half-doped manganites is controlled by the combination of metastability, an inhomogeneous high field state, and cation disorder. We study this non-equilibrium problem via real space Monte Carlo on a disordered strong coupling model appropriate to the manganites. We reproduce the variation of the switching fields with the mean ionic radius r_A and cation disorder σ_A , and demonstrate how the experimental features arise from the proximity of several phases in the Landau free energy landscape. Our prediction for the field melted state is consistent with a growing body of experimental evidence.

The manganites owe their fame to the ‘colossal magnetoresistance’ effect, whereby an applied magnetic field strongly suppresses the resistance of the material. The most extreme version of this happens when the field can actually induce an insulator-metal transition (IMT). This occurs in the low bandwidth half doped manganites, *e.g.*, $\text{Pr}_{0.5}\text{Ca}_{0.5}\text{MnO}_3$, that are typically charge ordered (CO) insulators with CE magnetic order [1–3]. The CE-CO-I state is transformed to a ferromagnetic metal (FM-M) by an applied field through a first order phase transition. The magnetic field induced conversion of the CE order to FM, and the crucial resistive switching, involve several subtleties which are only gradually being appreciated [4–14]. These include the surprising difference between the melting fields in two lanthanide (Ln) families, namely the Ca [4] and the Sr [5,6] families; the smallness of the field melting energy scales [4–7]; and the *spatial character* of field induced melting and its relation to structural disorder [8–12]. We expand on these issues below.

(i) The phase boundary between the CE and FM phase is first order, so metastable states exist on either side. This leads to hysteresis, and the switching fields are decided by *non-equilibrium effects*, not free energy balance. (ii) While trapping into metastable states is expected in a first order transition, an applied field leads to *new equilibrium states* which are not simple continuation of the zero field state. In particular, it is increasingly apparent that the field induced conducting state is an *inhomogeneous*

FM-M, a percolative metal with a finite volume fraction of charge ordered regions [8–12]. Finally, (iii) the field induced switching and inhomogeneous metallicity play out on a structurally disordered background. One expects the CO-I state to be more stable in narrow band systems. While this is true in the Ca based manganites [4], where the cation size mismatch σ_A is small, it is completely opposite in the Sr based systems [5,6]. The more insulating system can be driven metallic *easier* in the presence of disorder!

These three actors, metastability, field induced inhomogeneity, and pinning disorder, enrich and complicate the field melting problem. There is no understanding of their interplay in the field induced IMT, and the non-equilibrium physics of the manganites.

We study a coupled electron-spin-lattice model [15] appropriate to the manganites, in two dimensions (2D). For parameters where the FM-M and CE-CO-I phases are in proximity, we discover the following. (i) In the ‘clean’ limit, the forward (CE to FM) and reverse (FM to CE) switching fields, h_c^+ and h_c^- respectively, increase rapidly with decreasing bandwidth (BW), and below a threshold BW the field cannot melt the CO. This explains the results in the ‘clean’ Ca based manganites. (ii) The switching fields are dramatically affected by disorder: $h_c^\pm \rightarrow 0$ as the bandwidth reduces, as in the Sr manganites, even though the CO is notionally stronger. (iii) The field melted state in the narrow band case is inhomogeneous even without

arXiv:0801.2054v2 [cond-mat.str-el] 20 Mar 2009

disorder - at finite field the system exists as a patchwork of metallic and CO regions, and the ‘metallicity’ is of percolative origin. Recent experiments have indeed verified coexistence of FM-M and CO-I, *e.g.*, in $\text{La}_{0.5}\text{Ca}_{0.5}\text{MnO}_3$ [11] and $\text{Pr}_{0.5}\text{Sr}_{0.5}\text{MnO}_3$ [9, 10], and the phase volumes are tunable depending on the field cooling protocol.

We consider the field response of a model H_0 that we had studied earlier [15] to capture phase competition. Our model is:

$$\begin{aligned}
 H &= H_0 - \mu \hat{N} + \sum_i \epsilon_i n_i - h \sum_i S_{iz} \\
 H_0 &= \sum_{\langle ij \rangle \sigma} t_{\alpha\beta}^{ij} c_{i\alpha\sigma}^\dagger c_{j\beta\sigma} - J_H \sum_i \mathbf{S}_i \cdot \boldsymbol{\sigma}_i + J \sum_{\langle ij \rangle} \mathbf{S}_i \cdot \mathbf{S}_j \\
 &\quad - \lambda \sum_i \mathbf{Q}_i \cdot \boldsymbol{\tau}_i + \frac{K}{2} \sum_i \mathbf{Q}_i^2
 \end{aligned} \quad (1)$$

H_0 involves two e_g levels per Mn, with nearest neighbour hopping $t_{\alpha\beta}^{ij}$ [16], and Hund’s coupling J_H between the e_g electrons and the t_{2g} derived core spins. We assume a 2D square lattice. The e_g electrons have a coupling λ to Jahn-Teller phonons, while the core spins have an antiferromagnetic (AF) superexchange J between them. The stiffness of the phonon modes is K , μ is the chemical potential, and the magnetic field, $\mathbf{h} = \hat{z}h$, couples to the core spins. The ‘phonons’ are treated in the adiabatic limit and provide a *static* distortion background for the electrons. The core spins are also treated as classical [17]. At half doping, $n = 0.5$, the clean model has a variety of phases of which we are interested in the CE-CO-I phase and its response to a magnetic field. Cation disorder leads to ‘site disorder’ due to the potential generated by the randomly located rare earth and alkaline earth ions, and ‘bond disorder’ in t_{ij} and J . We retain only the local random potential since it couples to the electron density and has a direct impact on charge order. It was recently shown [18] that while off-diagonal disorder is crucial for obtaining the spin glass phases at half doping, it is diagonal disorder that plays a dominant role in weakening and eventual disruption of the CO state. We model the potential ϵ_i seen at the Mn site as binary distribution $P(\epsilon_i) = \frac{1}{2}(\delta(\epsilon_i - \Delta) + \delta(\epsilon_i + \Delta))$ with variance Δ^2 . For H_0 we use $J_H/t \rightarrow \infty$, and set $|\mathbf{S}_i| = 1$. $t = 1$ is set as the reference energy scale and we also set $K = 1$. We restrict ourselves to $J/t = 0.12$. The chemical potential μ is adjusted to keep the electron density at $n = 1/2$ which is also $x = 1 - n = 1/2$.

We use the travelling cluster (TCA) based Monte Carlo method [19] to solve the coupled electron-spin-phonon system above. Classical Monte Carlo techniques have been extensively used in literature [20] to study first order transitions and the associated hysteresis. We will explore the dependence of the melting process on bandwidth (λ/t), disorder (Δ/t), and temperature T/t . The experimental variation of bandwidth (via r_A) implies simultaneous change in λ/t , J/t and Δ/t , while we have varied λ/t , J/t and Δ/t independently. Our primary variation is in λ/t

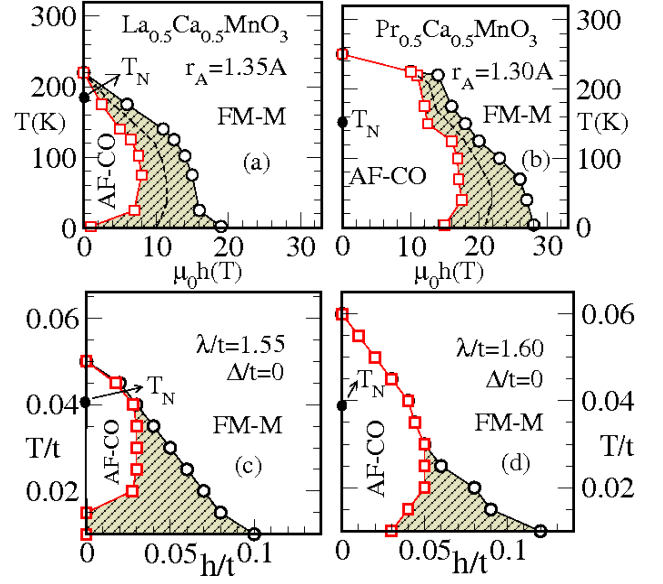


Fig. 1: Colour online: $h - T$ phase diagrams. (a)-(b) Experimental phase diagrams in (a) moderate BW $\text{La}_{0.5}\text{Ca}_{0.5}\text{MnO}_3$ and (b) narrow band $\text{Pr}_{0.5}\text{Ca}_{0.5}\text{MnO}_3$. Both materials have low cation disorder, $\sigma_A \sim 10^{-3}A^2$. (c)-(d) Our results for two values of λ/t and disorder $\Delta/t = 0$. The parameters are chosen to mimic the experimental regimes above (see text) in terms of hysteretic response. Both FM-M and AF-CO-I states are locally stable in the shaded region.

and, crudely, we compare this to experimental BW variation. We have commented on this in more detail elsewhere [21].

All our results are for cooling at $h = 0$ followed by field sweep. The ‘upper’ and ‘lower’ switching fields, h_c^\pm , in the hysteretic response refer to the resistive transitions.

The field induced melting of CO has been studied within mean field theory (MFT) earlier. For a model involving double exchange and Coulomb effects Mishra *et al.* [22] showed that suitable parameter choice could lead to a low $h_c \sim 6\text{T}$. Fratini *et al.* [23], considered a more elaborate model and worked out typical $h - T$ phase diagrams within MFT, and Cepas *et al.* [24] used a variational approach at $T = 0$ to estimate h_c . These studies, unfortunately, do not shed light on the spatial character of melting or the impact of disorder.

Let us first clarify the field melting and hysteresis in manganites with weak cation disorder. σ_A is small, $\sim 10^{-3}A^2$, in the lanthanide (Ln) family $\text{Ln}_{0.5}\text{Ca}_{0.5}\text{MnO}_3$ [4] so as reference we look at $\text{La}_{0.5}\text{Ca}_{0.5}\text{MnO}_3$ (LCMO), with a relatively large BW, and $\text{Pr}_{0.5}\text{Ca}_{0.5}\text{MnO}_3$ (PCMO), with a smaller BW. Fig.1.(a)-(b) reproduces the $h - T$ phase diagrams for these compounds from [4]. At low temperature h_c^+ is $\sim 20\text{T}$ for LCMO and $\sim 30\text{T}$ for PCMO. The field h_c^- , at which CO is *recovered* on field reduction, is, however, $< 1\text{T}$ in LCMO, but $\sim 15\text{T}$ in PCMO. $h_c^- \sim 0$ at low temperature in LCMO indicates that the FM-M is metastable *even at* $h = 0$, while at smaller BW (PCMO)

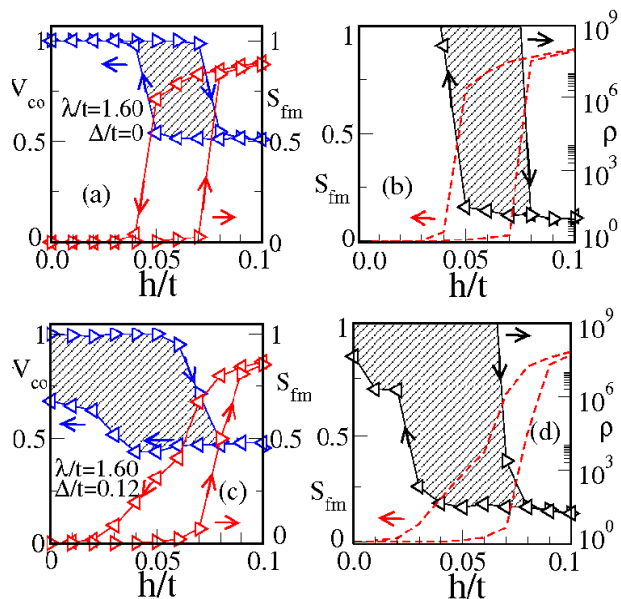


Fig. 2: Colour online: Response to field cycling at $\lambda/t = 1.6$ and $T/t = 0.02$. (a)-(b) Clean system $\Delta/t = 0$: (a) field response of the CO volume fraction (see text) and the FM structure factor S_{fm} , (b) the resistivity $\rho(h)$. (c)-(d) Corresponding results in the disordered case $\Delta/t = 0.12$. Shaded region is the hysteretic window. Contrast the abrupt switching in the clean limit with the broad crossover in the disordered case. Note, both the CO volume fraction and the FM magnetic structure factors are normalized to unity.

the FM-M is no longer metastable at $h = 0$. The T_{CO} at $h = 0$ for these two systems are $\sim 220\text{K}$ and 250K respectively.

Panels (c)-(d) show $h - T$ phase diagrams computed by us at two couplings. For the lower value, $\lambda/t = 1.55$, $T_{CO}/t \sim 0.05$, while for $\lambda/t = 1.60$, $T_{CO}/t \sim 0.06$. Using a crude factor of $3/2$ to convert from 2D to 3D and setting $t \sim 0.25\text{eV}$, these would correspond to about 210K and 250K . More significantly, $\lambda/t = 1.55$, which is closer to the (FM-M CO-I) phase boundary, shows $h_c^- = 0$, akin to LCMO, while at $\lambda/t = 1.6$, h_c^- is finite and the FM-M state is no longer metastable at $h = 0$. Although our h_c^+ scales, $\sim 0.1t$, are larger than in experiments [25], the typical value $\frac{1}{2}(h_c^+ + h_c^-)$ varies roughly similarly in the experiments and theory, changing from 10T to 20T between LCMO and PCMO and $\sim 0.05t$ and $0.08t$ in Fig.1.(c)-(d). It is possible that including electron-electron interaction may reduce the melting fields somewhat [23] as mean field studies suggest. The $h - T$ phase diagram is derived from the evolution of the $\mathbf{q} = \{0, 0\}$ feature in the magnetic structure factor $S(\mathbf{q})$ and the ‘volume fraction’ V_{co} [26] of the CO phase.

Fig.2 shows these features at $\lambda/t = 1.6$ and $T/t = 0.02$. Fig.2.(a) shows the ‘switching’ of V_{co} and $S_{fm} = S(0, 0)$ on field cycling, for a clean system. The complementary switching in FM and CO volume fraction is sharp and simultaneous, along with the transition in resistivity $\rho(h)$

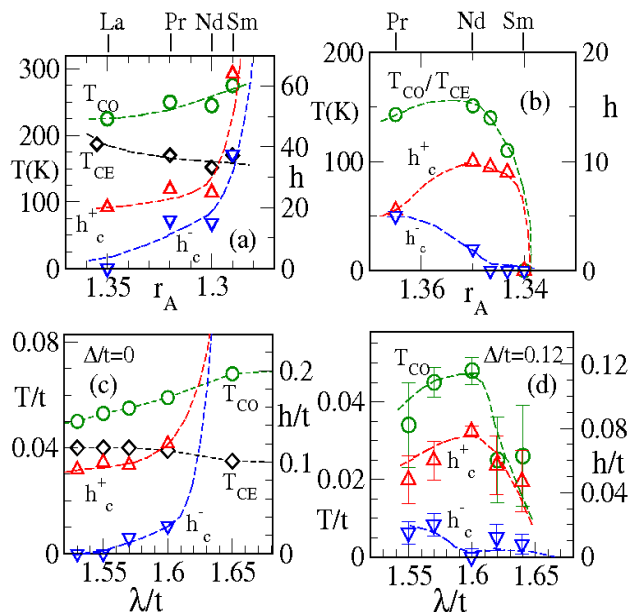


Fig. 3: Colour online: T_{CO} , and h_c^\pm at low T - comparing experiment and theory. (a)-(b) Data from experiments: (a) the $\text{Ln}_{0.5}\text{Ca}_{0.5}\text{MnO}_3$ family, with typical $\sigma_A \sim 10^{-3}A^2$, (b) the $\text{Ln}_{0.5}\text{Sr}_{0.5}\text{MnO}_3$ family with typical $\sigma_A \sim 10^{-2}A^2$. Notice the rapid increase in h_c^\pm with decreasing r_A at $r_A \sim 1.29 \text{ \AA}$ in (a), and the collapse of h_c^\pm with decreasing r_A at $r_A \sim 1.34 \text{ \AA}$ in (b). (c)-(d) Our results on the λ/t dependence of T_{CO} , T_{CE} and h_c^\pm . (c) Clean limit $\Delta/t = 0$, (d) disordered systems, $\Delta/t = 0.12$. The lines are a guide to the eye.

shown in Fig.2.(b). Notice the residual V_{co} in the field melted metallic state in Fig.2.(a). For a weakly disordered CO state, at $\Delta/t = 0.12$, Fig.2.(c) shows that the CO melts on increasing h , but fails to recover on downward sweep. The magnetism in Fig.2.(c) and $\rho(h)$ in Fig.2.(d) still show hysteresis but the transitions are quite broad. This suggests that the field induced ‘melting’ in the disordered case *occurs gradually*, unlike the abrupt switching in the clean case.

Using indicators as shown in Fig.1 and Fig.2 we made a comprehensive comparison between experiment and theory for the dependence of transition temperatures and low T melting fields on BW and disorder. Fig.3.(a) is data from the ‘low disorder’ $\text{Ln}_{0.5}\text{Ca}_{0.5}\text{MnO}_3$ [4] family, and Fig.3.(b), is for the moderate disorder $\text{Ln}_{0.5}\text{Sr}_{0.5}\text{MnO}_3$ [5] family. We compare these with our results on the λ/t dependence of T_{CO} and h_c^\pm in Fig.3.(c) and Fig.3.(d), with $\Delta/t = 0$ and $\Delta/t = 0.12$ respectively.

(A) In the clean limit, Fig.3.(a), T_{CO} increases with decreasing BW, T_{CE} decreases, and the fields h_c^\pm increase rapidly beyond $\text{Sm}_{0.5}\text{Ca}_{0.5}\text{MnO}_3$ (SCMO). A comparison of Fig.3.(a) with Fig.3.(c) shows that our results capture all the experimental trends in the clean limit. The increase in T_{CO} is due to the decrease in kinetic energy with decreasing r_A (increasing λ/t in our case), while T_{CE} is suppressed because CE magnetic order is also kinetic energy

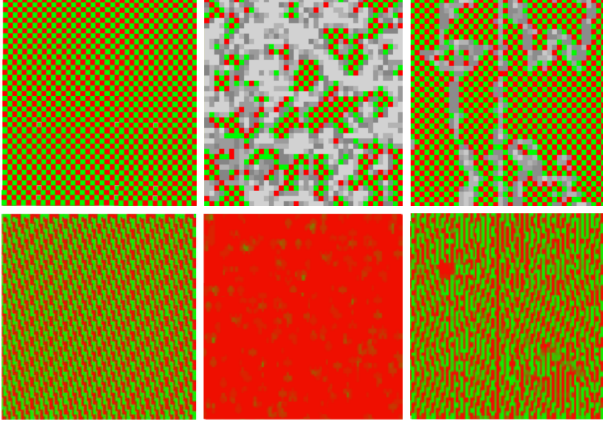


Fig. 4: Colour online: Spatial snapshots of local charge order (top row) and nearest neighbour magnetic correlation $\mathbf{S}_i \cdot \mathbf{S}_j$ (bottom row) on field cycling, $\lambda/t = 1.55$, $\Delta/t = 0$, $T/t = 0.02$. $h = 0$ (left) initial state, $h > h_c^+$ (center), and $h = 0$ (right) after the field sweep. The lattice size is 40×40 . In the bottom panel the red bonds are FM the green bonds are AF. In the top panel grey regions imply metallic regions and the red and green regions are the $0.5 - \delta$ and $0.5 + \delta$ onsite charge densities.

driven and gives way to a ‘G type’ $\{\pi, \pi\}$ phase at large λ/t . The increasing separation of T_{CO} and T_{CE} implies that the charge order becomes progressively independent of CE magnetic order with decreasing BW, and so *less responsive to an applied field*. This is precisely what one observes for h_c^\pm in Fig.3.(a) & (c), where below a critical BW the CO no longer melts! In fact for $\lambda/t > 1.60$ we observe that the high field state is FM-CO and not FM-M. The magnetic phase change no longer drives a resistive transition.

(B) For the disordered family, Fig.3.(b), T_{CO} and h_c^\pm decrease rapidly as we head towards small BW $\text{Sm}_{0.5}\text{Sr}_{0.5}\text{MnO}_3$ (SSMO). Our results in Fig.3.(d) probe BW variation at disorder $\Delta/t = 0.12$, and capture the correct dependence. The fall in T_{CO} at large λ/t is due to the competition between the ‘stiffness’ ($K_{eff}(\lambda)$, say) of the CO state, which weakens at large λ/t [27], and the pinning effect of the random potential ϵ_i . This is similar to the random field Ising model [28] where the exchange (J_{eff}) serves the role of our ‘stiffness’ and the random field (h_i) is akin to ϵ_i . As is well known, long range order is lost below a threshold for $J_{eff}/\sqrt{\langle h_i^2 \rangle}$, equivalent to our K_{eff}/Δ . The weakening and ultimate destruction of the zero field CO state with decreasing r_A (or t/λ) automatically suppresses the melting fields h_c^\pm . The non monotonic character of T_{CO} and h_c , with a reduction also at the large BW end, is due to the presence of the competing FM-M phase at $\lambda/t < 1.5$.

While the trends are well captured, let us compare the experimental T_{CO} scales with theory. At the ‘large’ BW end, $r_A \sim 1.36A$, ‘clean’ LCMO has $T_{CO} \sim 220\text{K}$, while

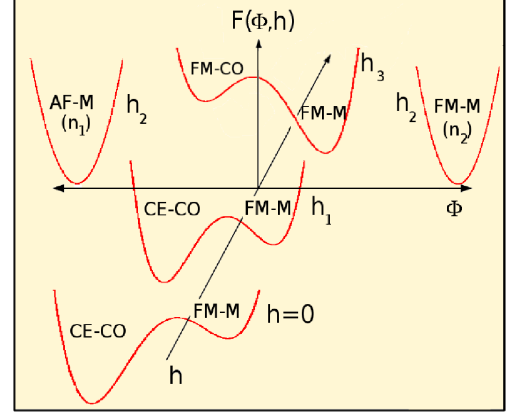


Fig. 5: Colour online: Landau landscape. We plot the free energy $F(\phi, h)$, where ϕ is the ‘order parameter’ (on the x axis) and can have FM-M, CE-CO-I, AF-M, or AF-CO character. h increases from h_1 to h_3 (on the y axis). We have not shown the metastable FM-CO state, for $h \sim h_2$, to avoid cluttering.

‘disordered’ $\text{Pr}_{0.5}\text{Sr}_{0.5}\text{MnO}_3$ (PSMO) has a suppressed $T_{CO} \sim 150\text{K}$. If we identify $\lambda/t \sim 1.55$ crudely as the equivalent, the clean T_{CO} is $\sim 0.055t \sim 225\text{K}$, and the ‘disordered’ T_{CO} is $\sim 0.035t \sim 145\text{K}$. The peak T_{CO} is $\sim 160\text{K}$ in Fig.3.(b) and it is $\sim 0.05t \sim 200\text{K}$ in theory. Given that we are solving a 2D model and have not fine tuned parameters the correspondence is reasonable.

The thermodynamic indicators, however, do not reveal the spatial character of the ‘melted’ state, while Fig.2.(a) & (c) suggest something unusual: there is finite CO phase fraction in the ‘FM-M’! Our map of the density field in Fig.4 reveals how the system is spatially organised. The lower panels show that the CE phase transforms to a FM at large field (and only partially recovers CE order on reverse sweep) but the large h density field is *strongly inhomogeneous*. The middle panel, top row, shows charge modulated ‘minority’ regions in a homogeneous background, surviving way past the CE \rightarrow FM transition. For the parameter values in Fig.4, and overall for $\lambda/t < 1.6$, the ‘high field’ state is a *percolative* metal. Beyond $\lambda/t = 1.6$ it is an insulating FM-CO.

The peculiar high field state requires us to examine the various phases that ‘compete’ in the manganites around $x \sim 0.5$ at finite h . At $h = 0$ the $x = 0.5$ CE-CO-I is separated from a FM-M phase at lower x , and an AF-M phase at larger x , by windows of PS [15]. However, beyond a small threshold field a homogeneous $x = 0.5$ state is no longer possible [21] and the $x = 0.5$ system breaks up into either (a) $x < 0.5$ FM-M and $x > 0.5$ AF-M patches, for $\lambda/t < 1.6$, or (b) $x < 0.5$ FM-CO and $x > 0.5$ AF-M patches for $\lambda/t > 1.6$. These intermediate field states evolve, respectively, into a homogeneous FM-M or FM-CO state at large h . While the finite h equilibrium state is complicated by PS, field sweep experiments (and our

simulation) also probe the existence of metastable states in which the system can get trapped. Fig.5 summarises the situation at $\lambda/t \sim 1.55$ in terms of a Landau free energy schematic. At $h = 0$ the CE-CO-I is the absolute minimum while the FM-M is metastable (ref Fig.1.(c)). This continues to finite h , we show a typical field $h = h_1$. At $h = h_2(\lambda)$ the $x = 0.5$ state phase separates into AF-M and FM-M, and there is also a metastable FM-CO. Finally, at some $h = h_3(\lambda)$ the equilibrium state is a homogeneous FM-M but the continuing presence of the low energy metastable FM-CO state would affect all low T field sweep experiments.

To conclude, we have clarified how non-equilibrium effects and disorder control the field driven conductance switching and insulator-metal transition in the half doped manganites. We discover that the field induced conducting state is spatially inhomogeneous, even in the absence of quenched disorder. Our results on the $h-T$ phase diagram and the spatial character of the melted state address existing results and growing body of spatially resolved data.

We acknowledge use of the Beowulf cluster at HRI.

REFERENCES

- [1] TOKURA Y. (EDT) *Colossal Magnetoresistive Oxides*, Gordon and Breach, Amsterdam (2000).
- [2] For a review see TOKURA Y., Rep. Prog. Phys. **69**, 797 (2006).
- [3] AKAHOSHI D., UCHIDA M., TOMIOKA Y., ARIMA T., MATSUI Y., and TOKURA Y., Phys. Rev. Lett. **90**, 177203 (2003).
- [4] RESPAUD M., LLOBET A., FRONTERA C., RITTER C., BROTO J. M., RAKOTO H., GOIRAN M. and GARCIA-MUNOZ J. L., Phys. Rev. **B 61**, 9014 (2000).
- [5] TOKURA Y., KUWAHARA H., MORITOMO Y., TOMIOKA Y. and ASAMITSU A., Phys. Rev. Lett. **76**, 3184 (1996).
- [6] KUWAHARA H., MORITOMO Y., TOMIOKA Y., ASAMITSU A., KASAI M., KUMAI R. and TOKURA Y., Phys. Rev. **B 56**, 9386 (1997).
- [7] TOMIOKA Y., ASAMITSU A., MORITOMO Y., KUWAHARA H., and TOKURA Y., Phys. Rev. Lett. **74**, 5108 (1995).
- [8] WU W. D., ISRAEL C., HUR N., PARK S., CHEONG S.-W., and LOZANNE A. D., Nat. Mater., **5**, 881 (2006)
- [9] KUMAR K., PRAMANIK A. K., BANERJEE A., CHADDAH P., ROY S. B., PARK S., ZHANG C. L., and CHEONG S-W., Phys. Rev. **B 73**, 184435 (2006).
- [10] PRAMANIK A. K. and BANERJEE A., arXiv:0803.0085.
- [11] CHADDAH P., KUMAR K. and BANERJEE A., Phys. Rev. **B 77**, 100402 (2008).
- [12] TROKINER A., VERKHOVSKII S., YAKUBOVSKII A., KUMAGAI K., MONOD P., MIKHALEV K., BUZLUKOV A., FURUKAWA Y., HUR N., and CHEONG S-W., Phys. Rev. **B 77**, 134436 (2008).
- [13] KAWANO H., KAJIMOTO R., YOSHIZAWA H., TOMIOKA Y., KUWAHARA H. and TOKURA Y., Phys. Rev. Lett. **78**, 4253 (1997).
- [14] KIRSTE A., GOIRAN M., RESPAUD M., VANAKEN J., BROTO J. M., RAKOTO H., VON ORTENBERG M., FRONTERA C. and GARCIA-MUNOZ J. L., Phys. Rev. **B 67**, 134413 (2003).
- [15] PRADHAN K., MUKHERJEE A., and MAJUMDAR P., Phys. Rev. Lett. **99**, 147206 (2007).
- [16] The detailed orbital and ij dependence is given in [15].
- [17] The validity of the classical approximations is studied in, e.g. DAGOTTO E., YUNOKI S., MALVEZZI A. L., MOREO A., HU J., CAPPONI S., POILBLANC D., and FURUKAWA N., Phys. Rev. **B 58**, 6414 (1998) and GREEN A. C., Phys. Rev. **B 63**, 205110 (2001).
- [18] KUMAR S. and KAMPF A., Phys. Rev. Lett. **100**, 076406 (2008).
- [19] KUMAR S. and MAJUMDAR P., Eur. Phys. J. **B 50**, 571 (2006).
- [20] LANDAU D. P. and BINDER K., Phys. Rev. **B 17**, 2328 (1978), BINDER K. and LANDAU D. P., Phys. Rev. **B 30**, 1477 (1984), RAO M., KRISHNAMURTHY H. R., and PANDIT R., Phys. Rev. **B 42**, 856 (1990); J. Appl. Phys. **67**, 5451 (1990), LI B. L., LIU X. P., FANG F., ZHU J. L., and LIU J.-M., Phys. Rev. **B 73**, 014107 (2006),
- [21] MUKHERJEE A. and MAJUMDAR P., arXiv:0811.3563.
- [22] MISHRA S. K., PANDIT R. and SATPATHY S., Phys. Rev. **B 56**, 2316 (1997).
- [23] FRATINI S., FEINBERG D. and GRILLI M., Eur Phys. J. **B 22**, 157 (2001).
- [24] CEPAS O., KRISHNAMURTHY H. R. and RAMAKRISHNAN T. V., Phys. Rev. Lett. **94**, 247207 (2005).
- [25] This smallness of h_c is due to the proximity of the FM-M and CE-CO-I phases *over a large part of parameter space* in 3D. Within our 2D framework the FM-M and CE-CO-I neighbour each other only over a narrow window, and are otherwise separated by a magnetic phase ('A-2D') with ordering at $\mathbf{q} = \{0, \pi\}, \{\pi, 0\}$. This increases $\mathcal{E}_{FM} - \mathcal{E}_{CO}$ and thus the h_c . Since we have not fine tuned parameters so that $\mathcal{E}_{FM} \approx \mathcal{E}_{CO}$ our typical h_c are somewhat large.
- [26] Our CO volume fraction is a measure of the local CO correlation, obtained by essentially counting the number of sites on the lattice which are correctly coordinated to form a local (π, π) charge order. We prefer this 'short range' measure since it is useful in both 2D and 3D, and correlates with the transport. Features depending on long range order will not survive the effect of disorder in 2D.
- [27] MUKHERJEE A. and MAJUMDAR P., arXiv:0811.3746.
- [28] SEPPALA E. T. and ALAVA M. J., Phys. Rev. **E 63**, 066109 (2001).